batteries

Article

Electrical Modeling and Impedance Spectra of Lithium-Ion Batteries and Supercapacitors

Jin-Yong Bae

Department of Electric Vehicle Engineering, Dongshin University, Naju 58245, Republic of Korea; bjy@dsu.ac.kr; Tel.: +82-61-330-7652

Abstract: In this study, electrical models for cylindrical/pouch-type lithium Li-ion batteries and supercapacitors were investigated, and the impedance spectra characteristics were studied. Cylindrical Li-ion batteries use Ni, Co, and Al as the main materials, while pouch-type Li-ion batteries use Ni, Co, and Mn as the main materials. Herein, 2600–3600 mAh 18650-type cylindrical Li-ion batteries, 5000 mAh 21700-type cylindrical Li-ion batteries, 37–50.5 Ah pouch-type Li-ion batteries, and a 2.7 V, 600 F supercapacitor are compared and analyzed. For a cylindrical Li-ion battery, the R_S value of a battery with a protection device (circular thermal disc cap) is in the range of 14–38 mΩ. For the 18650-type cylindrical Li-ion battery with a protection device, the R_S value of the battery is between 48 and 105 mΩ, and the protection device increases the R_S value by at least 33 mΩ. A good Li-ion battery exhibits R_S. Moreover, it has small overall R_P and C_P values. For the 21700-type cylindrical Li-ion battery with a protection device, the R_S value of the battery is 25 mΩ. For the pouch-type Li-ion battery, the R_S value of the battery is between 0.86 and 1.04 mΩ. For the supercapacitor, the R_S value of the battery is between 0.4779 and 0.5737 mΩ. A cylindrical Li-ion battery exhibits a semicircular shape in the impedance spectrum, due to the oxidation and reduction reactions of Li ions, and the impedance increases with a slope of 45° in the complex plane, due to the Z_W generated by Li ion diffusion. However, for a pouch-type Li-ion battery, the impedance spectrum exhibits a part of the semicircular shape, due to the oxidation and reduction reactions of Li ions, and the Z_W generated by Li ion diffusion does not appear. In a supercapacitor, the oxidation and reduction reactions of ions do not appear at all, and the Z_W generated by Li ion diffusion does not occur.

Keywords: impedance spectrum; Li-ion battery; supercapacitor; cylindrical battery; pouch battery

check for updates

Citation: Bae, J.-Y. Electrical Modeling and Impedance Spectra of Lithium-Ion Batteries and Supercapacitors. *Batteries* **2023**, *9*, 160. https://doi.org/10.3390/batteries9030160

Academic Editors: Zexiang Shen, Linfei Lai, Catia Arbizzani and Carlos Ziebert

Received: 22 December 2022
Revised: 23 February 2023
Accepted: 3 March 2023
Published: 8 March 2023

1. Introduction

Recently, as the importance of batteries as energy storage devices has increased, various studies have been conducted on various characteristics and electrical modeling of lithium-ion batteries [1–18] and supercapacitors [6,19–26].

In addition, research on the impedance change of the batteries and the interpretation of the characteristics based on frequency injection from high to low frequencies, based on the battery's impedance spectra, have been conducted [5–11,27–48].

This study investigates the electrical equivalent models and impedance spectra of cylindrical/pouch-type lithium Li-ion batteries and supercapacitors, based on various battery models. Figure 1 displays the simplest battery model, which comprises the battery voltage (E_B), the battery equivalent series resistance (R_S), and the battery open circuit voltage (V_B) [1].

Chan and Sutanto [1] proposed a Thevenin battery model, which is a more practical battery model, as shown in Figure 2.

The Thevenin battery model comprises the battery voltage (E_B), the battery equivalent series resistance (R_S), a battery parallel resistance (R_P), a battery parallel capacitor (C_P), and the battery open circuit voltage (V_B).

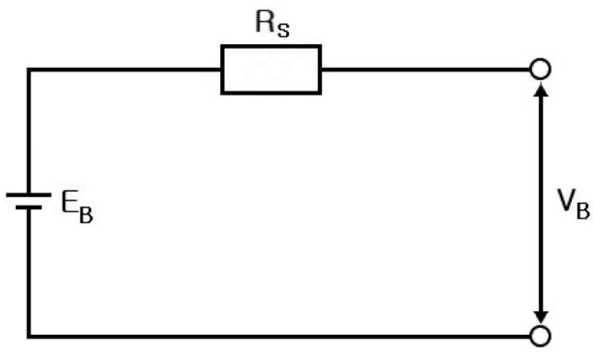

Figure 1. Simple battery model [1].

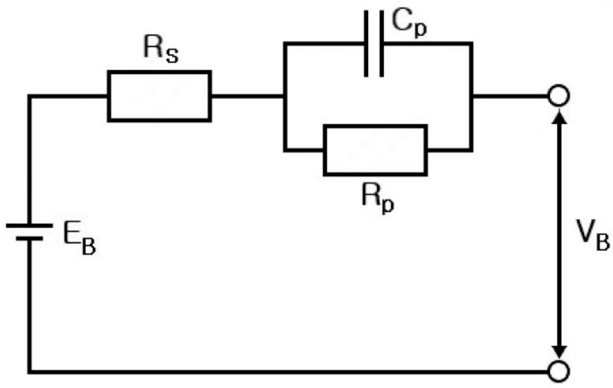

Figure 2. Thevenin battery model [1].

Additionally, the battery parallel resistance (R_P) represents the nonlinear resistance generated due to the contact resistance of the electrolyte [1]. Sims et al. [2] proposed the following equation to represent the dynamic characteristics of the battery [2]:

$$E_B = V_B - \left(R_S - \frac{K}{SOC} \right) i_{tb} \tag{1}$$

where K is the polarization constant, i_{tb} is the battery discharge current, and SOC is the state of charge.

The dynamic characteristics of the battery are characterized by considering SOC, K, and i_{tb} [2].

Ziyad et al. [3] and Margaret and Ziyad [4] proposed an improved battery model, which is shown in Figure 3. The improved battery model comprises E_B, R_P, and C_P; particularly, the variable resistor (R_c, R_d) and the diode (D_1, D_2) are arranged such that nonlinearity is afforded during charging and discharging. Moreover, the model includes a typical battery element [3,4].

In Figure 3, R_{PX} is the battery variable parallel resistance, R_C is the variable resistance when charging the battery, and R_d is the variable resistance when discharging the battery.

Recently, life prediction and performance analyses of the Li-ion batteries and supercapacitors used in electric vehicles, personal mobility vehicles, and energy storage systems (ESS) are being increasingly performed. Buller et al. [5,6] introduced a variable frequency for Li-ion batteries and supercapacitors, and based on this, proposed this study for analyzing their characteristics in the complex plane. Their method reduces the time required to perform the characteristic analysis of Li-ion batteries and supercapacitors, which is traditionally performed by charging and discharging Li-ion batteries and supercapacitors over long periods of time. Advantageously, it can analyze the basic characteristics of batteries within a very short time [5,6].

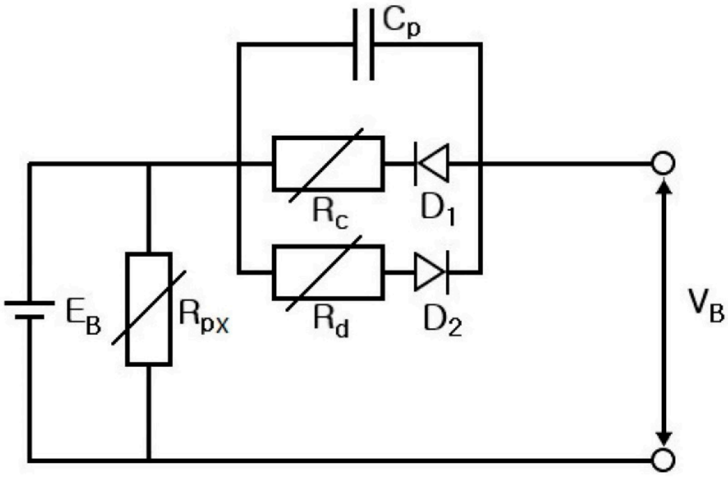

Figure 3. Improved battery model [3,4].

Electrical and mathematical models for cylindrical Li-ion batteries, pouch-type Li-ion batteries, and supercapacitors have been investigated [5–11]. By actually measuring the impedance spectrum in the state of being charged and discharged, the battery characteristics can be experimentally analyzed and compared. Subsequently, changes in the actual performance of cylindrical Li-ion batteries, pouch-type Li-ion batteries, and supercapacitors can be objectively observed, and the performance characteristics of electric vehicles, personal mobility vehicles, and ESS can be analyzed. This study suggests a method for quick and objective verification and analysis.

2. Electrical Modeling of Cylindrical Li-Ion Batteries

Figure 4 displays the impedance spectrum of a cylindrical Li-ion battery in the complex plane [6,8]. Cylindrical Li-ion batteries use Ni, Co, and Al as the main materials. In the impedance spectrum, the series inductor (L_S) of the cylindrical battery is located in the high-frequency region (f_{max}), and the part where the trace of the impedance spectrum and the real axis (Re Z) meet is the R_S of the cylindrical battery.

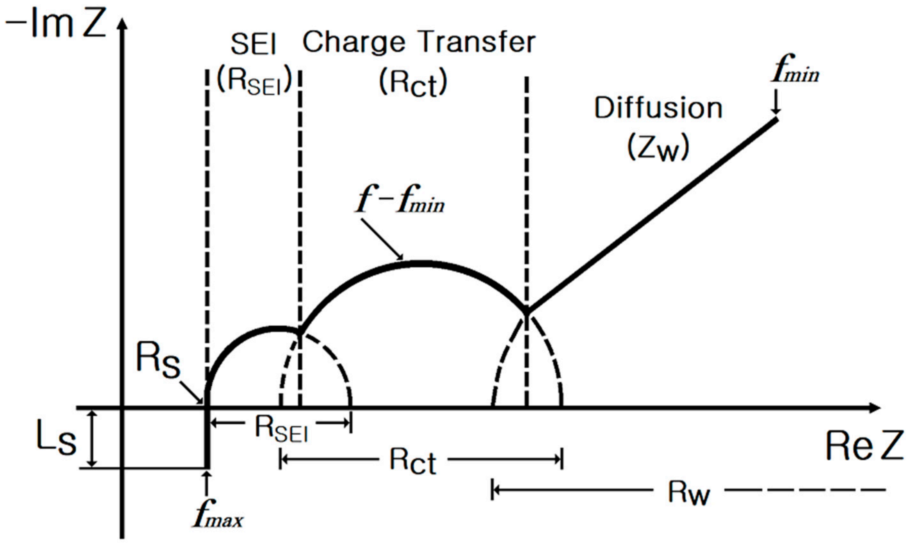

Figure 4. Complex plane diagram of the impedance spectrum of a cylindrical Li-ion battery [5,7].

In Figure 4, the small semicircle, which is expressed using the film resistance (R_{SEI}) and the capacitor (Q_{SEI}, α_{SEI}), corresponds to the charge transfer of the solid electrolyte interface (SEI) generated by the inner electrode. The Warburg impedance (Z_W), which is the diffusion region, denotes the diffusion of solid-state Li ions, and it increases with a slope of 45° in the complex plane [6,8]. Z_W can be expressed as follows [8,9]:

$$Z_W = \frac{1}{Q(j\omega)^n} = \frac{R_\omega}{\sqrt{j\omega}} \tanh\left(\sqrt{j\omega}\right) \quad (2)$$

where Q is the capacitor, ω is the angular frequency, and R_ω is the resistance at angular frequency.

Figure 5 depicts the electrical equivalent circuit of a cylindrical Li-ion battery.

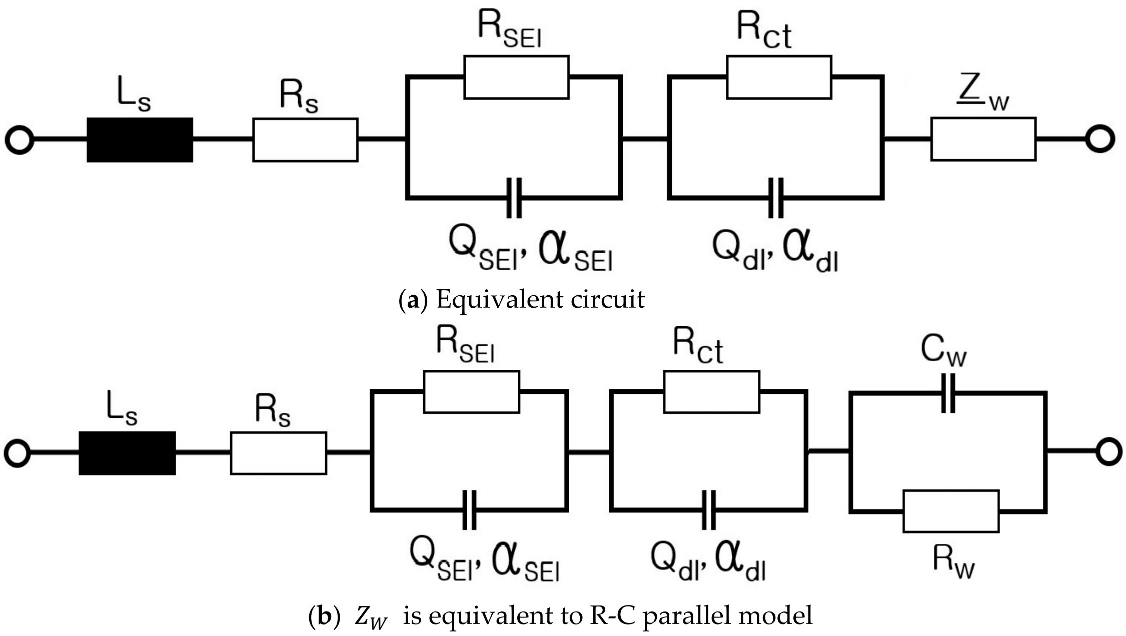

Figure 5. Electrical equivalent circuit of a cylindrical Li-ion battery.

For a cylindrical Li-ion battery, since the parallel plate battery is wound into a cylinder, the series inductor (L_S) is relatively larger than that for a pouch-type battery, and the R_S of the battery is arranged in series therewith.

The R_{SEI} and Q_{SEI}, α_{SEI} corresponding to charge transfer are arranged according to the SEI generated by the internal electrode of the Li-ion battery, and the charge transfer resistance (R_{ct}) representing the oxidation and reduction reactions of Li ions and a double layer (Q_{dl}, α_{dl}) are arranged. Furthermore, the Warburg impedance (Z_W) afforded by Li ion diffusion can be modeled as a resistor (R_W) and a capacitor (C_W). Particularly, the impedance spectrum of a cylindrical Li-ion battery in the complex plane shows that the first small semicircle is generated by the SEI, and the second large semicircle is generated by the oxidation and reduction reactions of Li ions. The diffusion of Li ions is a part of the large semicircle, and it increases with an inclination of 45° in the complex plane [5,7].

Based on Figure 5, the equivalent impedance for a cylindrical Li-ion battery can be expressed as follows [8–10].

$$Z(\omega) = j\omega L + R_s + \frac{R_{SEI}}{1 + R_{SEI} \cdot Q_{SEI}(j\omega)^{\alpha_{SEI}}} + \frac{R_{CT}}{1 + R_{CT} \cdot Q_{dl}(j\omega)^{\alpha_{dl}}} + \frac{1}{Q(j\omega)^n}$$

$$Z(\omega) = j\omega L + R_s + \frac{R_{SEI}}{1 + R_{SEI} \cdot Q_{SEI}(j\omega)^{\alpha_{SEI}}} + \frac{R_{CT}}{1 + R_{CT} \cdot Q_{dl}(j\omega)^{\alpha_{dl}}} + \frac{R_\omega}{\sqrt{j\omega}} \tanh\left(\sqrt{j\omega}\right) \quad (3)$$

Figure 6 shows the impedance spectrum in the complex plane, according to the SoC, in a cylindrical Li-ion battery. Figure 6 shows that as the SoC of the battery increases, the oxidation and reduction reactions of Li ions at the electrode material interface of the Li-ion battery gradually decrease, and thus, the size of the semicircle decreases.

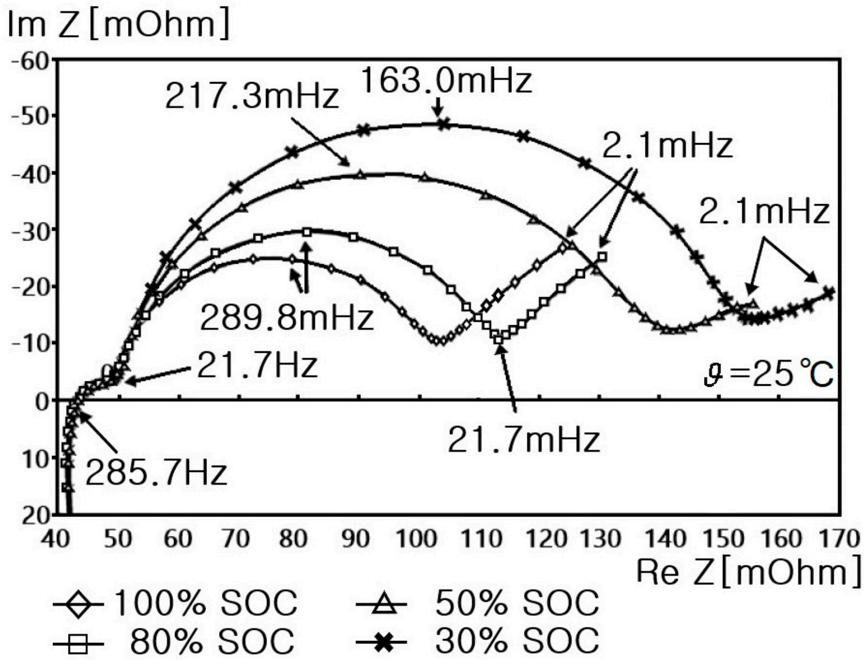

Figure 6. Impedance spectrum according to the SoC of a cylindrical Li-ion battery [5].

Figure 7 presents the impedance spectrum for a cylindrical Li-ion battery, according to the presence or absence of charging [5]. Figure 7 shows that the size of the semicircle also decreases as the oxidation and reduction reactions decrease when charging is not performed, compared to when charging at 1 A is performed [5].

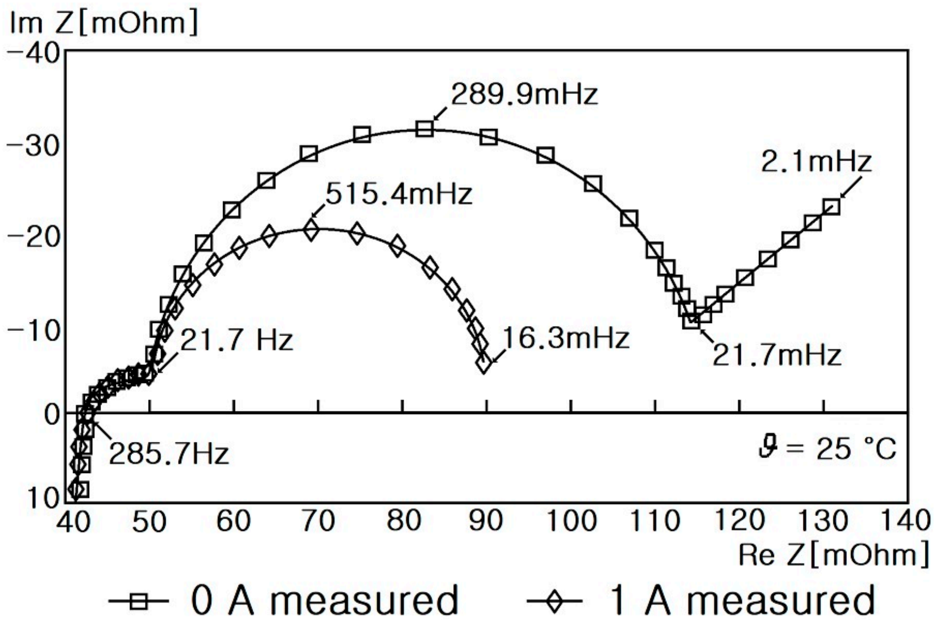

Figure 7. Impedance spectrum according to the presence or absence of charging for a cylindrical Li-ion battery [5].

3. Electrical Modeling of Pouch-Type Li-Ion Batteries

Figure 8 displays the electrical equivalent circuit of a pouch-type Li-ion battery in the complex plane [10].

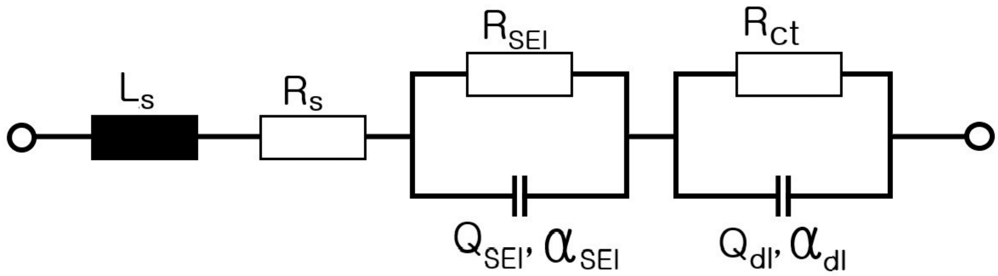

Figure 8. Electrical equivalent circuit of pouch-type Li-ion battery.

The pouch-type Li-ion battery uses cathode active material NMC (Ni, Co, and Mn) as the main materials. Since the overall structure of the battery has a parallel plate shape, it has a relatively small L_S compared to a cylindrical Li-ion battery.

It is placed in series with the L_S and R_S of the battery. The R_{SEI} and Q_{SEI}, α_{SEI} corresponding to the charge transfer are arranged according to the SEI generated by the internal electrode of the Li-ion battery, and the R_{ct} of the pouch-type Li-ion battery, representing the oxidation and reduction reactions of Li-ions and the double layer (Q_{dl}, α_{dl}), is the same as that of a cylindrical Li-ion battery.

However, the biggest difference in comparison to the cylindrical Li-ion battery, is that the Z_W, due to the Li ion diffusion, is not observed for the pouch-type Li-ion battery. Therefore, from Figure 8, the equivalent impedance for a cylindrical Li-ion battery can be expressed as follows [10]:

$$Z(\omega) = j\omega L + R_s + \frac{R_{SEI}}{1 + R_{SEI} \cdot Q_{SEI} (j\omega)^{\alpha_{SEI}}} + \frac{R_{CT}}{1 + R_{CT} \cdot Q_{dl} (j\omega)^{\alpha_{dl}}} \quad (4)$$

4. Electrical Modeling of Supercapacitors

Figure 9 presents the impedance spectrum of a supercapacitor in the complex plane [5,6,11]. Supercapacitors are based on carbon, and notably, they do not exhibit charge transfer of the SEI. Moreover, since oxidation and reduction reactions of ions do not occur, semicircular trajectories do not appear. However, due to the impedance of the supercapacitor, the impedance spectrum increases with a slope of 45°, and at very low frequencies, the impedance spectrum increases with a slope of 90°, like an ideal capacitor [6].

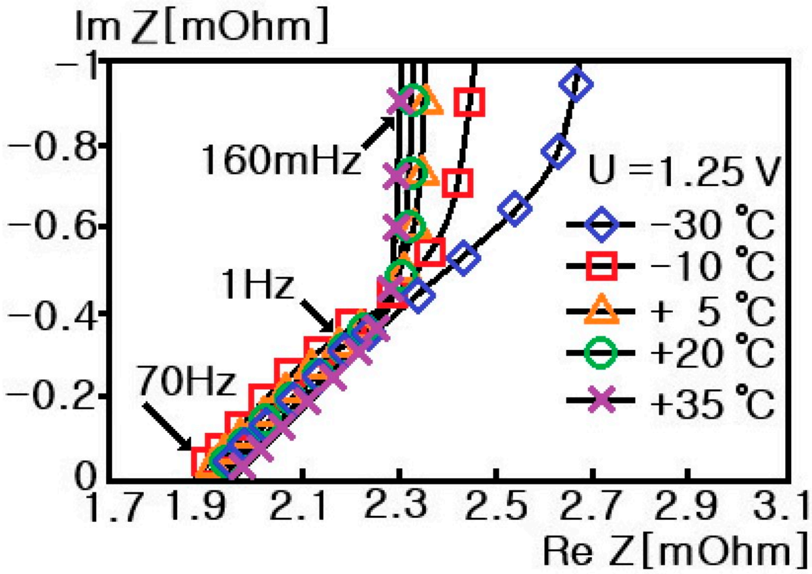

Figure 9. Impedance spectrum according to temperature of the supercapacitor [5,6].

Figure 10 shows the electrical equivalent circuit of a supercapacitor. The electrical equivalent circuit of a supercapacitor comprises L_S, R_S, and supercapacitor impedance ($\underline{Z}_P$). Z_P is afforded by the porosity of the supercapacitor electrode and can be expressed using Equation (5) [6,11].

$$\underline{Z}_P(j\omega) = \frac{\tau \cdot \cosh(\sqrt{j\omega\tau})}{C \cdot \sqrt{j\omega\tau}} \tag{5}$$

where, ω is the angular frequency, C is the capacitance of the supercapacitor, and τ is the independent parameter of temperature and voltage in supercapacitors.

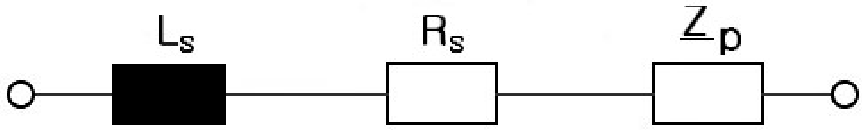

Figure 10. Electrical equivalent circuit of the supercapacitor [6].

Figure 11 displays the electrical equivalent model of $\underline{Z}_P$. $\underline{Z}_P$ is equivalent to a circuit wherein capacitor (C), and N capacitors $\left(\frac{C}{2}\right)$ and resistors $\left(\frac{\tau}{\pi^2}\frac{2}{n^2 \cdot C}\right)$, are connected in parallel.

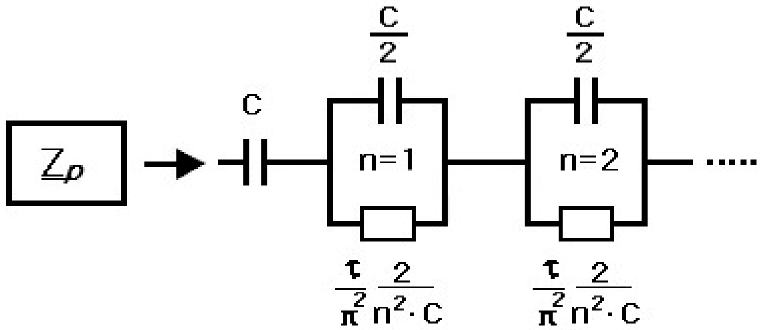

Figure 11. Electrical equivalent model of the supercapacitor impedance ($\underline{Z}_P$) [6].

Figure 12 shows the curve of τ [6]. Buller et al. [5,6,11] performed a simulation of the impedance spectrum of the supercapacitor in a complex plane according to Equation (4) and Figure 12. Figure 13 presents the theoretical model of the impedance spectrum of a supercapacitor with porous electrodes [5,6,11].

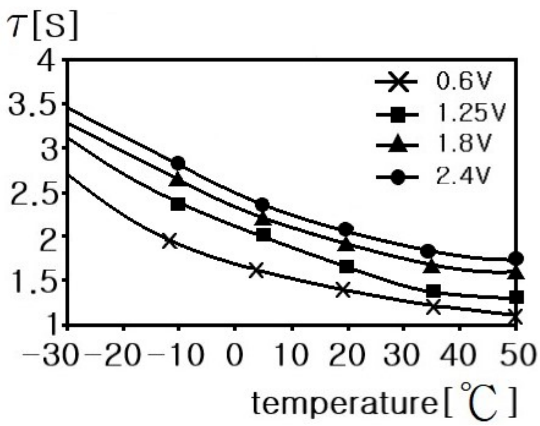

Figure 12. Curve of τ, which is an independent parameter of temperature and voltage in supercapacitors.

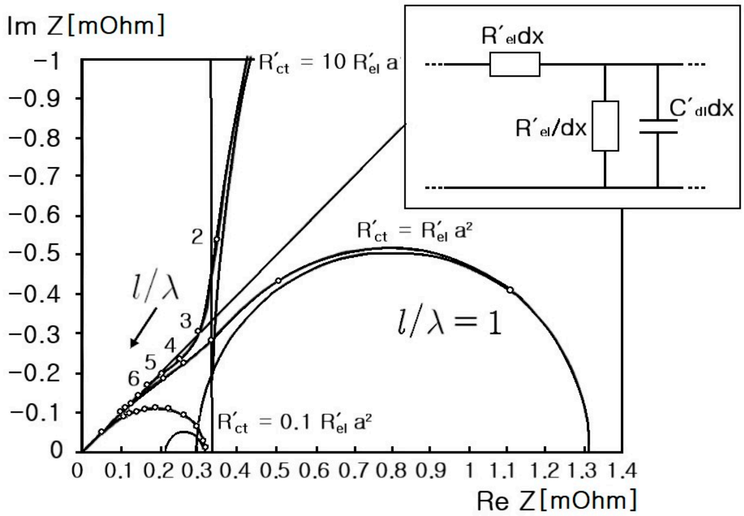

Figure 13. Theoretical model of the impedance spectrum of supercapacitors with porous electrodes [11].

where l is the length of the porous electrode, and λ is the wavelength.

Figure 13 shows a state with a small wavelength (λ) compared to the length (l) of the porous electrode. When $\frac{l}{\lambda} = 6 \sim 3$, the graph increases with a slope of 45°; when $\frac{l}{\lambda} < 3$, the graph increases with a slope of 90° [11].

5. Experimental Equipment and System

Table 1 shows the specifications of the Li-ion batteries and supercapacitor used herein.

Table 1. Specifications and parameters of the Li-ion batteries and supercapacitor.

Device Type of Energy Storage		Company	Quantity	Value
Cylindrical Li-ion battery	18650	① Fairman (Kor.)	Capacity	3500 mAh
			Type	Built-in protection device
			Color	Yellow
		② Fairman (Kor.)	Capacity	3400 mAh
			Type	Built-in protection device
			Color	Orange
		③ Fairman (Kor.)	Capacity	2600 mAh
			Type	Built-in protection device
			Color	Blue
		④ Fairman (Kor.)	Capacity	2600 mAh
			Type	Built-in protection device
			Color	Dark pink
		⑤ Samsung (Kor.)	Capacity	3000 mAh
			Type	Non-protection device
			Color	Pink

Table 1. *Cont.*

Device Type of Energy Storage		Company	Quantity	Value
		⑥ Samsung (Kor.)	Capacity	2900 mAh
			Type	Non-protection device
			Color	Blue
		⑦ Samsung (Kor.)	Capacity	2600 mAh
			Type	Non-protection device
			Color	Pink
		⑧ LG (Kor.)	Capacity	3500 mAh
			Type	Built-in protection device
			Color	Yellow/Black
		⑨ LG (Kor.)	Capacity	2600 mAh
			Type	Built-in protection device
			Color	Green
		⑩ LG (Kor.)	Capacity	2600 mAh
			Type	Non-protection device
			Color	Purple
		⑪ Panasonic (Jap.)	Capacity	3600 mAh
			Type	Built-in protection device
			Color	Green
		⑫ Shenzhen TrushFire Tech. (Chi.)	Capacity	3600 mAh
			Type	Built-in protection device
			Color	Black
		⑬ Shenzhen JiaChuangMing Tech. (Chi.)	Capacity	2600 mAh
			Type	Built-in protection device
			Color	Pink
	21700	⑭ Samsung (Kor.)	Capacity	5000 mAh
			Type	Built-in protection device
			Color	Black
Pouch-type Li-ion battery		Ⓐ Shenzhen Aoyouji Energy Electronics (Chi.)	Capacity	50.5 Ah
			Type	Non-protection device
			Color	BEV battery
		Ⓑ China Soundon New Energy (Chi.)	Capacity	48 Ah
			Type	Non-protection device
			Color	BEV battery
		Ⓒ A123System LLC (Chi.)	Capacity	37 Ah
			Type	Non-protection device
			Color	PHEV battery
Supercapacitor		Shenzhen Yedianxinbang Tech. (Chi.)	Capacity	600 F
			Rated voltage	DC 2.7 V

Impedance spectra were obtained for all 18 samples.

Figure 14 shows the Li-ion batteries and supercapacitor used in the experiments in this study.

Figure 14. Li-ion batteries and supercapacitor used in the experiment. (**a**) Cylindrical Li-ion batteries: 18650-type—13 samples; 21700-type—1 sample; total of 14 samples. (**b**) Pouch-type Li-ion batteries: size 300 × 100 × 10 mm; total of 3 samples. (**c**) Supercapacitor: diameter 60 × height 140 mm; total of 1 sample.

Figure 15 shows the impedance spectrum equipment and the experimental apparatus of the chamber, and Figure 16 shows the voltage and current waveforms obtained when measuring the impedance spectra.

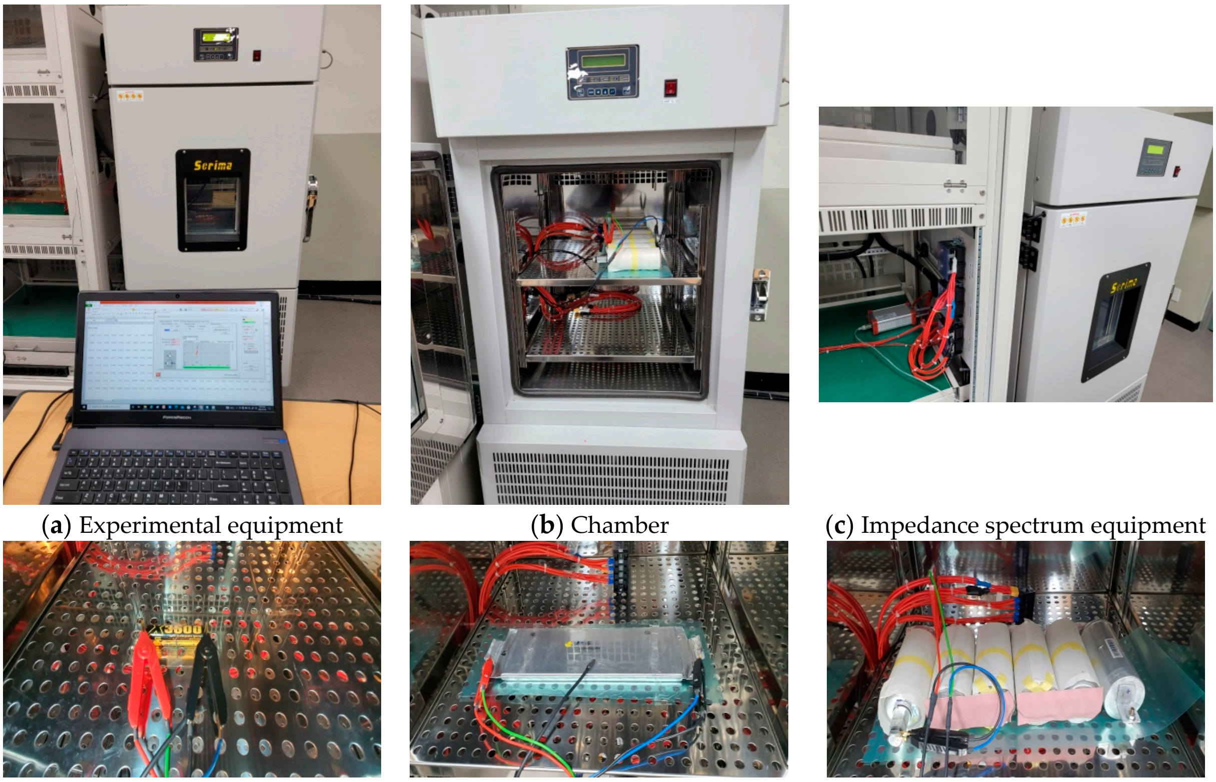

(**a**) Experimental equipment (**b**) Chamber (**c**) Impedance spectrum equipment

(**d**) Cylindrical Li-ion Battery (**e**) Pouch-type Li-ion battery (**f**) Supercapacitor

Figure 15. Experimental apparatus.

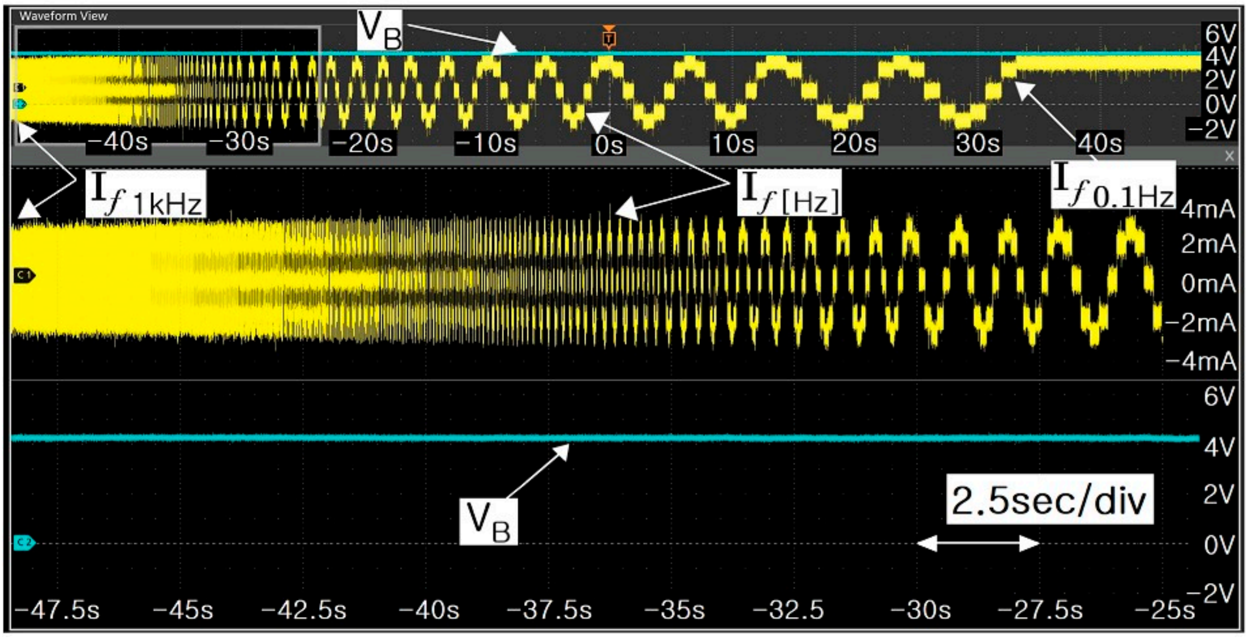

Figure 16. Voltage and current waveforms when measuring impedance spectrum.

The measurements were made using the battery measuring equipment of BRS Messtechnik GmbH (Strohberg 23, City of Stuttgart, Germany).

When measuring the impedance of the Li-ion batteries and supercapacitor, the impedance was measured while varying the frequency from 1 kHz to 0.1 Hz. The impedance spectra according to the charging and discharging states were measured and compared.

6. Experimental Results

6.1. Impedance Spectra of Cylindrical Li-Ion Batteries

Figure 17 shows the equivalent circuit of the batteries and supercapacitor used herein, as well as the values of R_S, R_P, and C_P. The electrical equivalent circuit can be represented by more precise modeling, for a cylindrical Li-ion battery (Figure 5), a pouch-type Li-ion battery (Figure 8), and a supercapacitor (Figure 10).

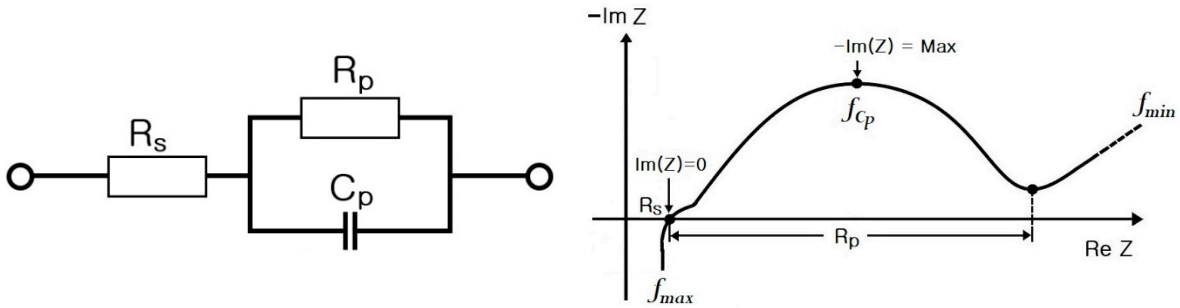

(**a**) Equivalent circuit used in the experiment (**b**) Typical curve fitting

Figure 17. Equivalent circuit and typical curve fitting.

However, in this experiment, it was equalized using the Thevenin battery model (Figure 2), and values can be defined as in Figure 17b.

Figure 18 compares the impedance spectra during charging and discharging of the 18650-type cylindrical Li-ion battery without a protective device. As shown in Figure 18a, the cylindrical Li-ion battery is equipped with a circular thermal disc cap, to prevent overvoltage or overcurrent.

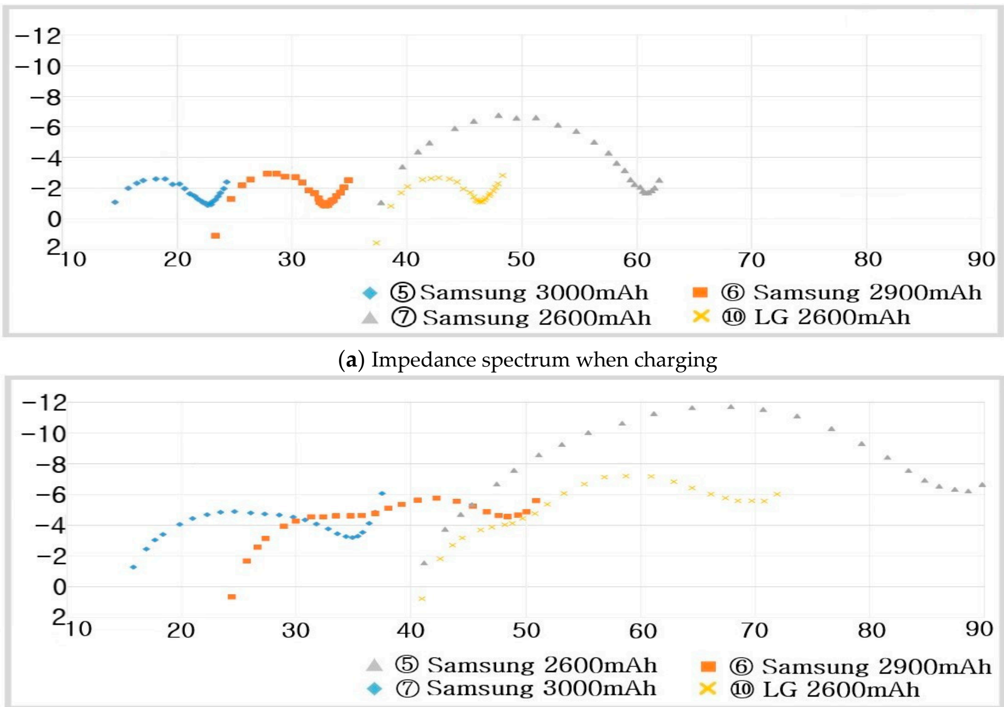

(**a**) Impedance spectrum when charging

(**b**) Impedance spectrum when discharging

Figure 18. Impedance spectra of 18650-type Li-ion batteries (non-protection device).

The impedance spectrum experiment comprised the following seven steps.

- Step 1: Cylindrical pouch-type Li-ion batteries and supercapacitors were prepared (Figure 14).
- Step 2: A chamber was used to keep the temperature constant at 25 °C. This is because the characteristics of batteries are temperature sensitive (Figure 15).
- Step 3: A sine wave frequency in the range of 1 kHz to 0.1 Hz was injected into the battery, through the impedance spectrum equipment (BRS Ltd.).
- Step 4: The impedance spectrum equipment acquired the following information from a reflected wave of the sinusoidal signal supplied: (1) injection frequency value (f), (2) RMS current value (I), and (3) RMS voltage value (V). The data were analyzed by shifting their frequency from 1 kHz to 0.1 Hz. The above data were graphed by dividing f.
- Step 5: The change in the parameters R, X_L, X_C, L, and C of the battery, with the battery frequency, was obtained from the following expressions:

$$\mathrm{R} = \frac{\mathrm{V}_{ac}}{\mathrm{I}_{ac}}\ [\Omega]$$

$$\mathrm{X}_L = \omega\ _L = 2\,\pi\, f\ \mathrm{L}\ [\Omega] \rightarrow \mathrm{L} = \frac{X_L}{2\,\pi\, f}$$

$$\mathrm{X}_C = \omega\ _C = -\frac{1}{2\,\pi\, f\ \mathrm{C}}\ [\Omega] \rightarrow \mathrm{C} = -\frac{1}{2\,\pi\, f\ X_C}$$

$$\mathrm{Z} = R + \mathrm{X}_L +\ \mathrm{X}_C\ [\Omega]$$

The above equation for V_{ac} and I_{ac} can be modified by using the complex function [38]: $\mathrm{j} = \sqrt{-1} = \exp\left(\frac{\mathrm{j}\pi}{2}\right)$:

$$\mathrm{V}_{ac} = \mathrm{V}_m \exp(j\omega)$$

$$\mathrm{I}_{ac} = \mathrm{V}_m \exp[j(\omega t - \varnothing)]$$

V_{ac} and I_{ac} satisfy Ohm's law for the AC circuit model. Therefore, the impedance $\mathrm{Z}(\omega)$ can be expressed as [38]:

$$\mathrm{Z}(\omega) = \frac{\mathrm{V}_{ac}(\omega)}{\mathrm{I}_{ac}(\omega)} = \frac{\mathrm{V}_m \exp(j\omega)}{\mathrm{I}_m \exp[j(\omega t - \varnothing)]} = \frac{\mathrm{V}_m}{\mathrm{I}_m} \exp(\mathrm{j}\varnothing)$$

$\mathrm{Z}(\omega)$ can be simplified using Euler's formula, $\exp(\mathrm{j}\varnothing) = \cos(\varnothing) + \mathrm{j}\sin(\varnothing)$

$$\mathrm{Z}(\omega) = \frac{\mathrm{V}_m}{\mathrm{I}_m} \exp(\mathrm{j}\varnothing) = \frac{\mathrm{V}_m}{\mathrm{I}_m}[\cos(\varnothing) + j\sin(\varnothing)] = \mathrm{Z}_0[\cos(\varnothing) + j\sin(\varnothing)]$$

By dividing the above equation into real and imaginary parts, the following equation can be obtained [38]:

$$\mathrm{Z}_{real} = \mathrm{Z}_0 \cos(\varnothing)\ \ :\mathrm{R(resistance)}$$

$$\mathrm{Z}_{img} = \mathrm{Z}_0 \sin(\varnothing):\ \mathrm{X}_L + \mathrm{X}_C$$

- Step 6: The values of R, X_L, X_C, L, and C, at frequencies from 1 kHz to 0.1 Hz, were determined, and graphs were drawn using the data.
- Step 7: R_S, R_P, and C_P are shown in Figure 17 and measured on the basis of the above data. Thus, the results in Figures 18–24 are experimental data, obtained by injecting a sine wave into a real battery, and based on the injection frequency, RMS current value (I), and RMS voltage value (V). In Figures 18–24, the units of the x-axis and y-axis are mΩ.

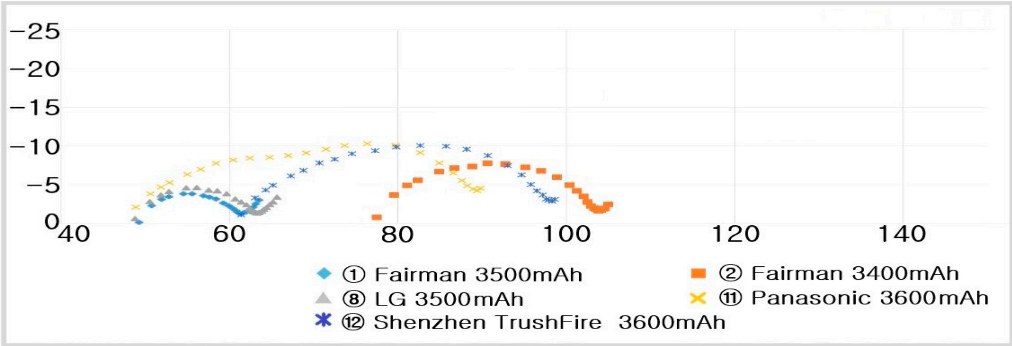

(**a**) Impedance spectrum when charging

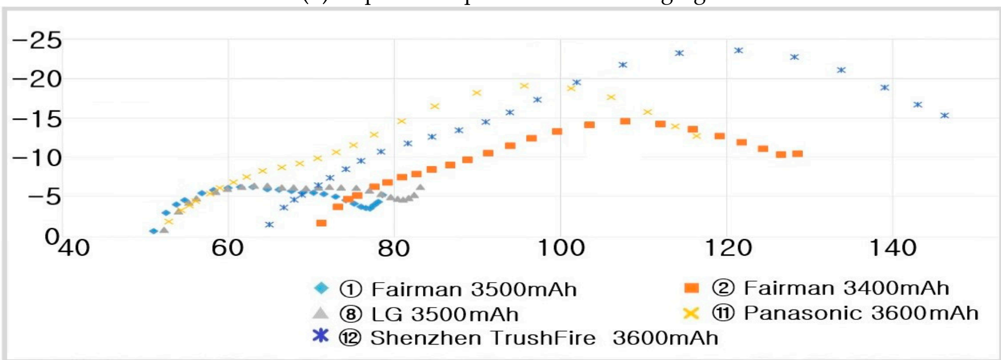

(**b**) Impedance spectrum when discharging

Figure 19. Impedance spectra of 18650-type (cylindrical 3400–3600 mAh) Li-ion batteries (built-in protection device).

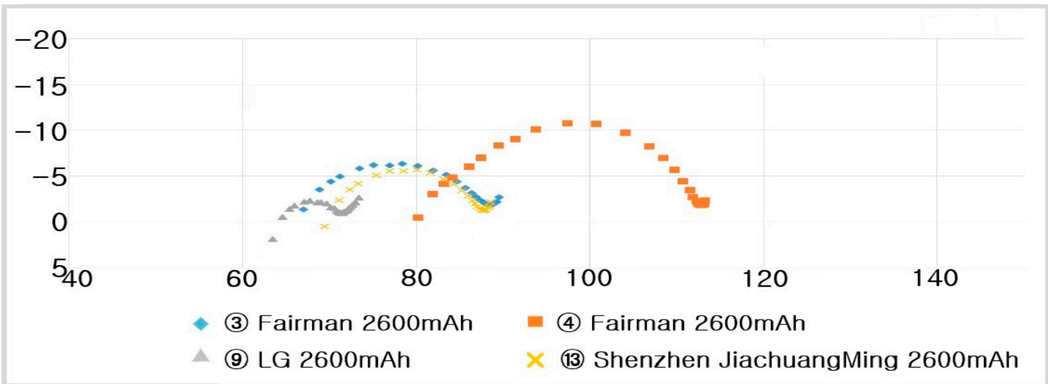

(**a**) Impedance spectrum when charging

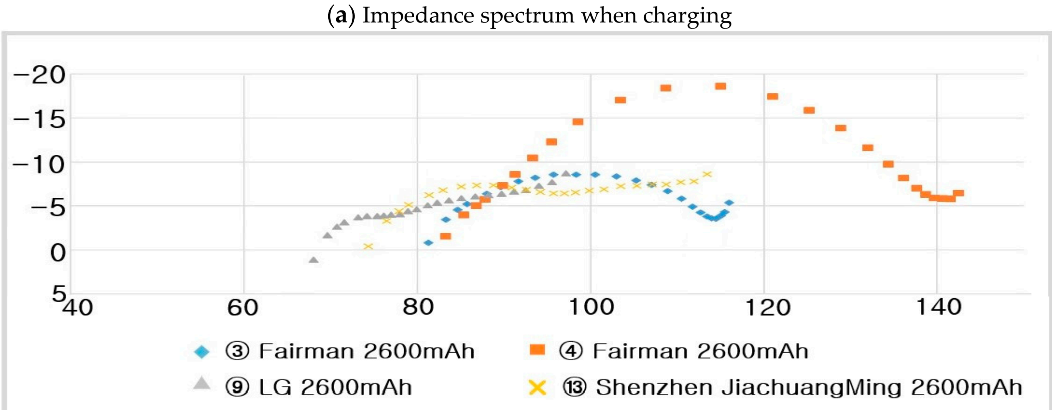

(**b**) Impedance spectrum when discharging

Figure 20. Impedance spectra of 2600 mAh 18650-type Li-ion batteries (built-in protection device).

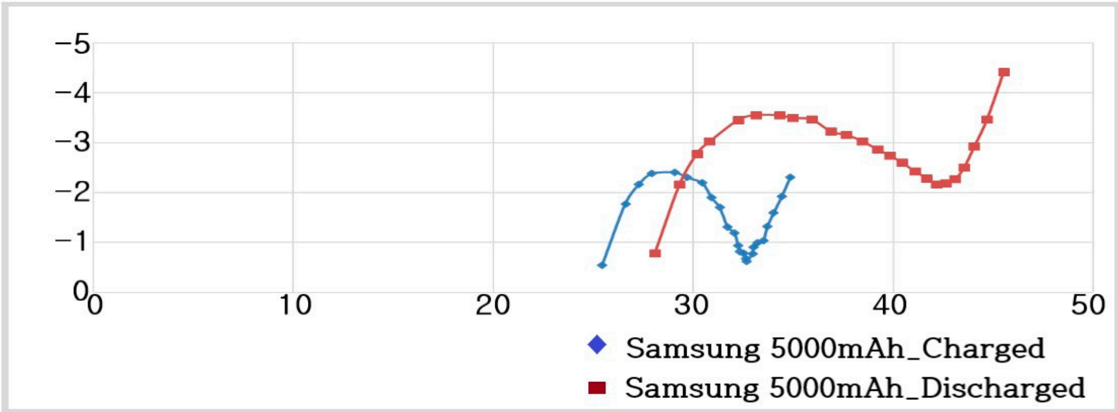

Figure 21. Impedance spectrum of 21700-type Li-ion Batteries (built-in protection device).

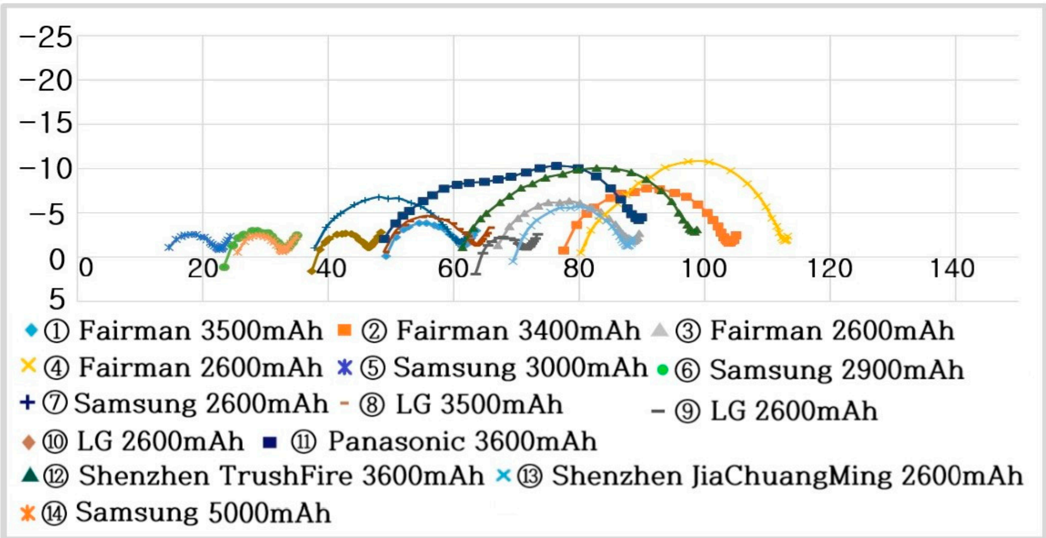

(**a**) Impedance spectrum when charging

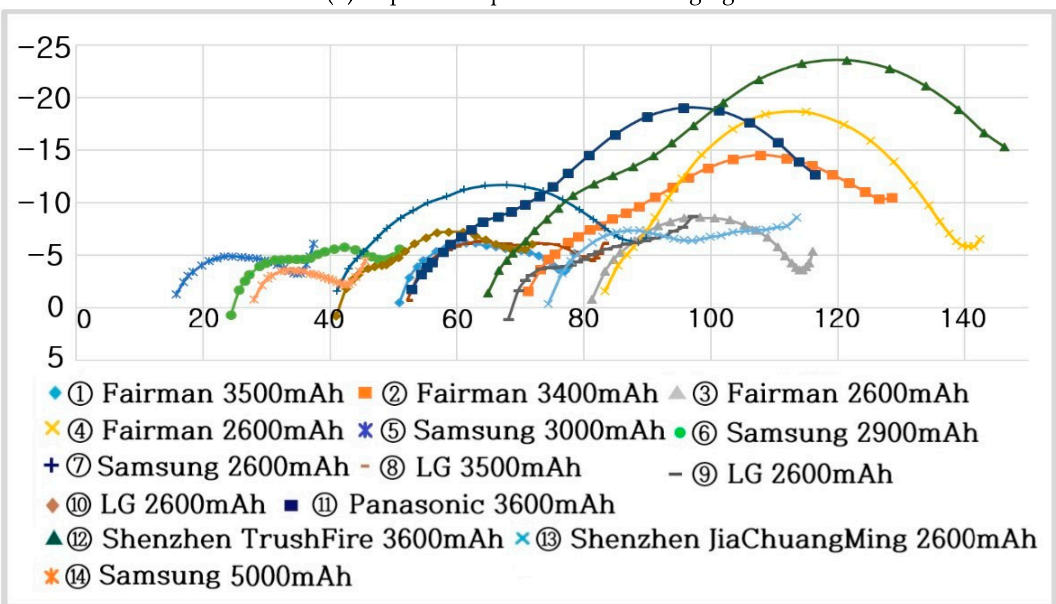

(**b**) Impedance spectrum when discharging

Figure 22. Impedance spectra of cylindrical Li-ion batteries.

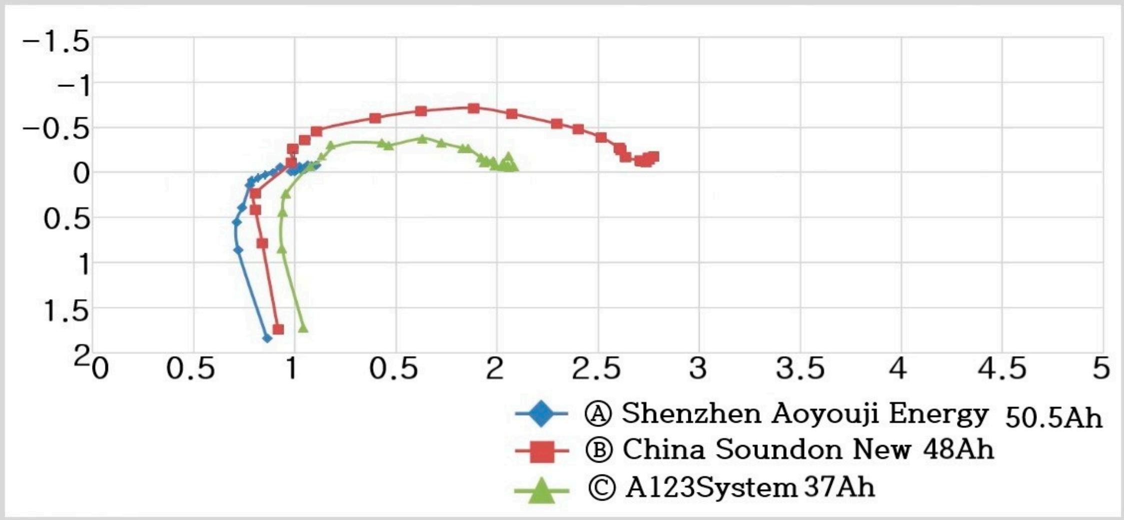

(**a**) Impedance spectrum when charging

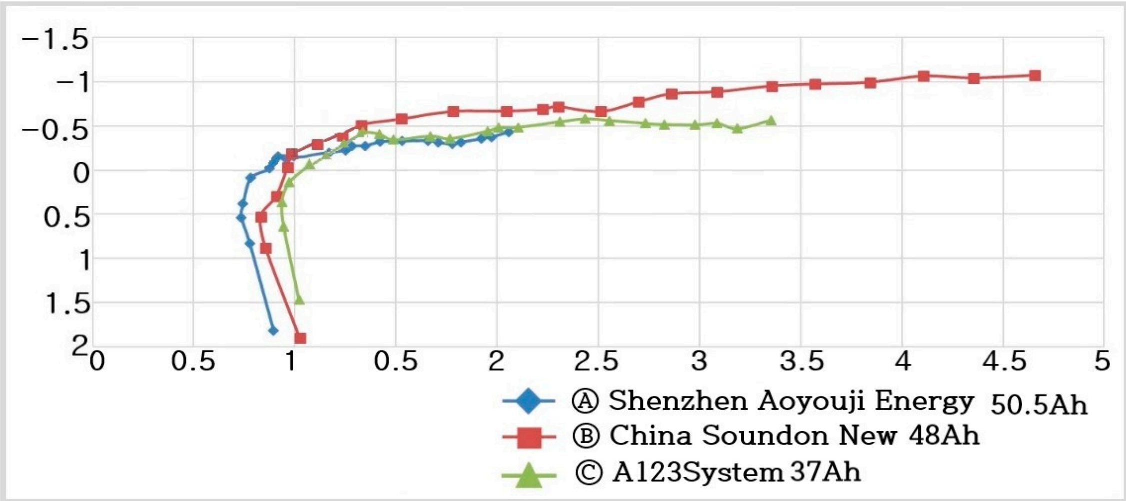

(**b**) Impedance spectrum when discharging

Figure 23. Impedance spectra of pouch-type Li-ion batteries.

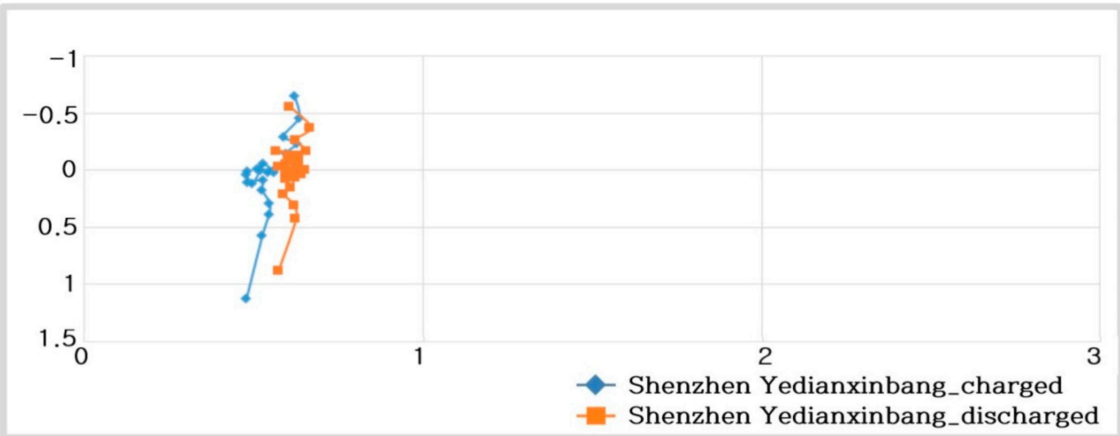

Figure 24. Impedance spectra of supercapacitor.

When such a protection device does not exist, the battery series impedance, 14–18 mΩ, represents a relatively low resistance value during charging. The experimental result in Figure 18 show that the R_S value was small when the capacity of the cylindrical Li-ion battery was large, and vice versa.

The battery equivalent series resistance (R_S) values of the 18650-type cylindrical Li-ion batteries, without the protection device, during charging are as follows:

- ⑤ Samsung 3000 mAh : $R_S = 14.5825$ mΩ
- ⑥ Samsung 2900 mAh : $R_S = 23.2917$ mΩ
- ⑦ Samsung 2600 mAh : $R_S = 37.7485$ mΩ
- ⑩ LG 2600 mAh : $R_S = 37.3298$ mΩ

Even for the Li-ion batteries with the same capacity, i.e., Samsung (⑦) and LG (⑩), the parallel impedance (R_P) and parallel capacitance (C_P) differ as follows:

- ⑦ Samsung 2600 mAh : $R_P = 22.9729$ mΩ, $C_P = 0.3525$ F
- ⑩ LG 2600 mAh : $R_P = 9.0120$ mΩ, $C_P = 0.6067$ F

For the 18650-type cylindrical Li-ion batteries without a protection element, a semicircle graph appears, due to the oxidation and reduction reactions of Li ions, and Li-ion batteries with smaller graphs exhibit better performances. Therefore, it can be predicted that the Samsung (⑦) Li-ion battery, with a smaller semicircle, will exhibit better performance than the LG (⑩) Li-ion battery, with a larger semicircle.

Figure 18b displays the impedance spectrum of a 18650-type cylindrical Li-ion battery without a protection element during discharge. The figure shows that the impedance of the battery increases as the battery discharges.

During discharge, the resistance increases, due to the oxidation and reduction reactions of Li ions, and the R_P values during the discharge are as follows.

- ⑤ Samsung 3000 mAh : $R_P = 19.1020$ mΩ
- ⑥ Samsung 2900 mAh : $R_P = 24.0597$ mΩ
- ⑦ Samsung 2600 mAh : $R_P = 47.4514$ mΩ
- ⑩ LG 2600 mAh : $R_P = 29.8173$ mΩ

The increase in the resistance value during the discharge of the battery can be explained by an increase in factors impeding the charge transfer in a Li-ion battery.

Comparing the Li-ion batteries of the same capacity, i.e., Samsung (⑦) and LG (⑩), the Samsung (⑦) battery with relatively small R_P and C_P has smaller battery impedance than the LG battery (⑩). The smaller the Li ion oxidation and reduction reactions, the better the exhibited properties.

Figure 19 compares the impedance spectra of charging and discharging of the 18650-type cylindrical 3400–3600 mAh Li-ion batteries equipped with protection devices. As shown in Figure 18, the R_S of the 18650-type Li-ion batteries without the protection device are in the range of 15–38 mΩ. As shown in Figure 19, the R_S of 18650-type Li-ion batteries with the protection device are in the range of 48–105 mΩ.

The use of a protective device (thermal disc cap) for preventing overvoltage or overcurrent is a major cause of the increase in R_S above the minimum of 33 mΩ.

Deciding the best battery among the various 18650-type cylindrical Li-ion batteries is essential. A battery with a relatively small R_S and R_P affords the best charge transfer characteristics during charging and discharging. A battery with a small C_P exhibits reduced oxidation and reduction reactions of Li ions when discharging.

As shown in Figure 19a, the R_S values of the 18650-type cylindrical Li-ion batteries with the protection device during charging are as follows.

- ⑧ LG 3500 mAh : $R_S = 48.7836$ mΩ
- ⑪ Panasonic 3600 mAh : $R_S = 48.8667$ mΩ
- ① Fairman 3500 mAh : $R_S = 49.2132$ mΩ
- ⑫ Shenzhen TrushFire 3600 mAh : $R_S = 61.4019$ mΩ
- ② Fairman 3400 mAh : $R_S = 77.4560$ mΩ

For the 3400–3600 mAh 18650-type Li-ion batteries with a protection device, the LG (⑧), Panasonic (⑪), and Fairman (①) batteries exhibited similar R_S values.

For the Shenzhen TrushFire (⑫) and Fairman (②) batteries, the R_S values were relatively large, 61 and 77 mΩ, respectively; thus, it can be predicted that the battery characteristics are somewhat deteriorated.

As shown in Figure 19a, for the Fairman (①), LG (⑧), and Panasonic (⑪) batteries with similar R_S values, the R_P values at each charge are as follows:

- ⑧ LG 3500 mAh : $R_P = 14.5156$ mΩ
- ⑪ Panasonic 3600 mAh : $R_P = 40.5615$ mΩ
- ① Fairman 3500 mAh : $R_P = 12.1129$ mΩ

Therefore, the Fairman (①) battery, with the smallest R_P, exhibited the best charge transfer characteristics during charging.

As shown in Figure 19b, the R_P and C_P values of the 18650-type cylindrical Li-ion batteries with a protection device during discharge are as follows:

- ⑧ LG 3500 mAh : $R_P = 28.7976$ mΩ, $C_P = 0.5290$ F
- ⑪ Panasonic 3600 mAh : $R_P = 63.5486$ mΩ, $C_P = 12.2790$ F
- ① Fairman 3500 mAh : $R_P = 26.0793$ mΩ, $C_P = 0.5439$ F
- ⑫ Shenzhen TrushFire 3600 mAh : $R_P = 81.3262$ mΩ, $C_P = 9.9237$ F
- ② Fairman 3400 mAh : $R_P = 55.2958$ mΩ, $C_P = 7.2934$ F

Even during discharging, the Fairman (①) battery exhibited the smallest R_P value; thus, it had the best charge transfer characteristics even during discharging. Additionally, the Fairman (①) battery had the smallest C_P value, of 6.1474 F; therefore, the oxidation and reduction reactions of the Li-ion battery will be reduced.

Figure 20 compares the impedance spectra during charging and discharging of 2600 mAh 18650-type cylindrical Li-ion batteries with a protection device. As shown in Figure 20a, the R_S values of the 18650-type cylindrical Li-ion batteries with a protection device during charging are as follows:

- ⑨ LG 2600 mAh: $R_S = 63.4390$ mΩ
- ③ Fairman 2600 mAh: $R_S = 66.9574$ mΩ
- ④ Fairman 2600 mAh: $R_S = 80.1501$ mΩ
- ⑬ Shenzhen JiaChuangMing 2600 mAh: $R_S = 69.4137$ mΩ

Figure 20 experimentally shows that the LG(⑨) battery exhibited the lowest R_S, R_P, and C_P values during charging. Therefore, it is predicted that the LG(⑨) battery has a small impedance when charging, and has excellent oxidation and reduction reactions.

Figure 21 shows the impedance spectra of a 21700-type Li-ion battery with a protection device. The R_S, R_P, and C_P values for the battery capacity during charging and discharging are as follows:

- (Charging) Samsung 5000 mAh: $R_S = 25.4537$ mΩ, $R_P = 7.2190$ mΩ, $C_P = 0.2645$ F
- (Discharging) Samsung 5000 mAh: $R_S = 28.0604$ mΩ, $R_P = 14.0903$ mΩ, $C_P = 0.4479$ F

Figure 21 displays the R_S value of the 21700-type Li-ion battery with protection device during discharging. In the figure, the R_P and C_P values increase overall. This denotes that the overall impedance of the battery increases and the oxidation and reduction reactions of Li ions increase.

Figure 22 displays the impedance spectra of the 18650- and 21700-type cylindrical Li-ion batteries. Recently, various companies have started selling Li-ion batteries with varying capacities, but it is difficult to confirm which battery is the best. Accurately determining the performance of a Li-ion battery only by the capacity (mAh) indicated on the surface is difficult.

If the R_S, R_P, and C_P values during charging are small overall, the values of R_S, R_P, and C_P do not significantly change even at the time of discharging. Cylindrical Li-ion batteries exhibit a semicircular shape due to their oxidation and reduction reactions, and it was experimentally confirmed that the Z_W afforded by Li ion diffusion increases at a slope of 45° in the complex plane.

6.2. Impedance Spectra of Pouch-Type Li-Ion Batteries

Figure 23 shows the impedance spectra of pouch-type Li-ion batteries.

As shown in Figure 23a, the R_S value when charging pouch-type batteries without a protection device are as follows:

- Ⓐ Shenzhen Aoyou vji Energy 50.5 Ah : $R_S = 0.8625$ mΩ
- Ⓑ China Soundon New Energy 48 Ah : $R_S = 0.9151$ mΩ
- Ⓒ A123System 37 Ah : $R_S = 1.042$ mΩ

It can be seen that pouch-type lithium-ion batteries showed a clear difference in the change of the impedance spectrum curve in the low-frequency region during charging and discharging. In particular, in the case of pouch-type lithium-ion batteries, the resistance, R, value increases in the low-frequency region during discharge, and the Z_W afforded by Li ion diffusion does not appear at all.

- Ⓐ-1 Shenzhen Aoyou vji Energy 50.5 Ah charging range of R: 0.722–1.181 mΩ
- Ⓐ-2 Shenzhen Aoyou vji Energy 50.5 Ah discharging range of R: 0.725–2.021 mΩ
- Ⓑ-1 China Soundon New Energy 48 Ah charging range of R: 0.728–2.758 mΩ
- Ⓑ-2 China Soundon New Energy 48 Ah discharging range of R: 0.729–4.199 mΩ
- Ⓒ-1 A123System 37 Ah charging range of R: 0.921–2.174 mΩ
- Ⓒ-2 A123System 37 Ah discharging range of R: 0.923–3.328 mΩ

The overall comparison of the cylindrical and pouch-type Li-ion batteries is as follows:

- 18,650 Cylindrical Li-Ion Battery (protected): 3400–3600 mAh $\triangleright$ $R_S = 48$–77 mΩ
- 18,650 Cylindrical Li-Ion Battery (protected): 2600 mAh $\triangleright$ $R_S = 63$–80 mΩ
- 18,650 Cylindrical Li-Ion Battery (unprotected):

$$2600\text{–}3000\ \text{mAh} \triangleright R_S = 14\text{–}38\ \text{m}\Omega$$

- 21,700 Cylindrical Li-Ion Battery (protected): 5000 mAh $\triangleright$ $R_S = 25$ mΩ
- Pouch-type Li-Ion Battery (unprotected): 37–50.5 Ah $\triangleright$ $R_S = 0.86$–1.04 mΩ

A pouch-type Li-ion battery basically has considerably smaller R_S than a cylindrical Li-ion battery, and the current capacity supplied by the battery is very good. For a pouch-type Li-ion battery, as the current increases, the R_S decreases.

The most fundamental difference between the pouch-type and cylindrical Li-ion batteries is that in the pouch-type batteries, only a part of the semicircular shape appears due to the oxidation and reduction reactions of Li ions, and the Z_W afforded by Li ion diffusion does not appear at all.

6.3. Impedance Spectrum of a Supercapacitor

Figure 24 illustrates the impedance spectrum of a supercapacitor.

As shown in Figure 24, the capacity of the supercapacitor is 600 F, and the R_S value is as follows:

- (Charging) Shenzhen Yedianxinbang 500 F : $R_S = 0.4779$ mΩ
- (Discharging) Shenzhen Yedianxinbang 500 F: $R_S = 0.5737$ mΩ

For the supercapacitor, the impedance spectrum increases with a slope of nearly 90°. The R_S of the supercapacitor is smaller than that of a pouch-type Li-ion battery, and the characteristics of the supercapacitor are substantially more similar to those of an ideal energy storage device, compared to the characteristics of the Li-ion batteries considered.

Table 2 summarizes the R_S, R_P, and C_P values of the Li-ion batteries and supercapacitor.

Table 2. R_S, R_P, and C_P values of Li-ion batteries and supercapacitor.

Cell Type			Charging 4.1–4.2 V			Charging 2.5–3.0 V		
			R_S[mΩ]	R_P[mΩ]	C_P[F]	R_S[mΩ]	R_P[mΩ]	C_P[F]
CYLINDRER	18650	① Fairman 3500 mAh Built-in protection	49.2132	12.1129	0.4140	50.9349	26.0793	0.5439
	18650	② Fairman 3400 mAh Built-in protection	77.4560	26.3065	0.4286	71.1773	55.2958	7.2934
	18650	③ Fairman 2600 mAh Built-in protection	66.9574	21.5832	0.5269	81.2983	33.1674	0.8552
	18650	④ Fairman 2600 mAh Built-in protection	80.1501	32.5909	0.6811	83.2599	58.2183	0.8534
	18650	⑤ Samsung 3000 mAh Non-protection	14.5825	8.0615	0.4300	15.7654	19.1020	0.9763
	18650	⑥ Samsung 2900 mAh Non-protection	23.2917	9.5717	0.3764	24.3366	24.0597	12.5382
	18650	⑦ Samsung 2600 mAh Non-protection	37.7485	22.9729	0.3525	41.1192	47.4514	1.9968
	18650	⑧ LG 3500 mAh Built-in protection	48.7836	14.5156	0.3427	52.2040	28.7976	0.5290
	18650	⑨ LG 2600 mAh Built-in protection	63.4390	8.0161	0.6920	68.0641	29.1099	182.175
	18650	⑩ LG 2600 mAh Non-protection	37.3298	9.0120	0.6067	40.9606	29.8173	6.6918
	18650	⑪ Panasonic 3600 mAh Built-in protection	48.8667	40.5615	4.6757	52.8348	63.5486	12.2790
	18650	⑫ Shenzhen TrushFire Tech. 3600 mAh Built-in protection	61.4019	36.9122	1.5803	64.9093	81.3262	9.9237
	18650	⑬ Shenzhen JiaChuangMing Tech. 2600 mAh Built-in protection	69.4137	18.2993	0.5883	74.3780	22.6098	0.4537
	21700	⑭ Samsung 5000 mAh Built-in protection	25.4537	7.2190	0.2645	28.0604	14.0903	0.4479
POUCH	Ⓐ Shenzhen Aoyouji Energy 50.5 Ah Non-protection		0.8625	-	41.2273	0.8941	-	3694.40
	Ⓑ China Soundon New Energy 48 Ah Non-protection		0.9151	-	14.6219	1.0247	-	1480.24
	Ⓒ A123System 37 Ah Non-protection		1.0420	-	19.6525	1.0209	-	2746.89
Supercapacitor Shenzhen Yedianxinbang 600 F			0.4779	-	2427.99	0.5737	-	2855.31

- The R_S value decreases in the following order: 18650-type cylindrical Li-ion battery > 21700-type cylindrical Li-ion battery > pouch-type Li-ion battery > supercapacitor.
- A cylindrical Li-ion battery with the smallest R_S, R_P, and C_p values exhibits the best characteristics.
- A cylindrical Li-ion battery exhibits a semicircular shape due to the oxidation and reduction reactions of Li ions, which increases with a slope of 45° in the complex plane due to the Z_W generated by Li ion diffusion.

- For a pouch-type Li-ion battery, a part of the semicircle shape appears due to the oxidation and reduction reactions of Li ions, but the Z_W afforded by Li ion diffusion does not appear.
- For a supercapacitor, no oxidation or reduction reactions of ions are observed, and the Z_W caused by Li ion diffusion hardly occurs, and its characteristics are similar to those of an ideal capacitor.

Figure 25 shows the discharge voltage and current waveforms of the cylindrical and pouch-type Li-ion batteries and supercapacitor. The voltage and current characteristics when discharging with a constant current (CC) were obtained using a discharge apparatus.

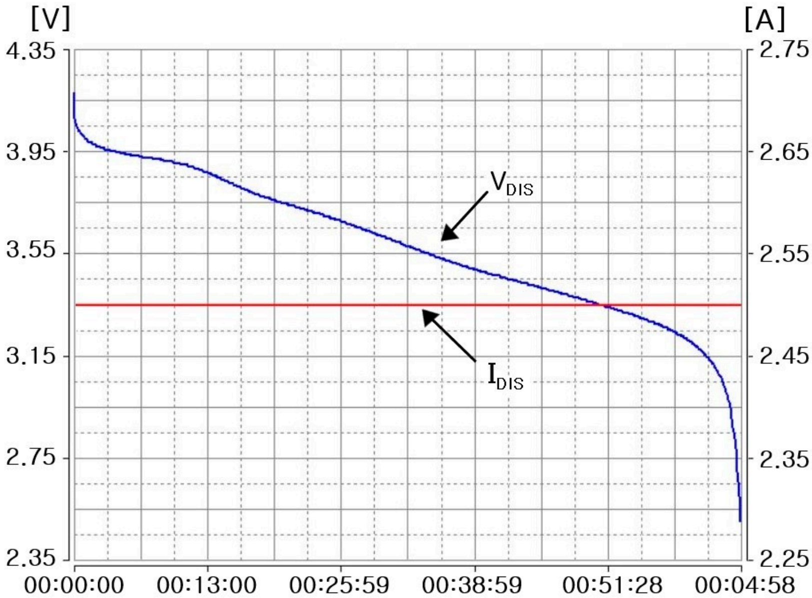

(**a**) Discharge voltage and current waveforms for a cylindrical Li-ion battery (⑥ Samsung 2900 mAh)

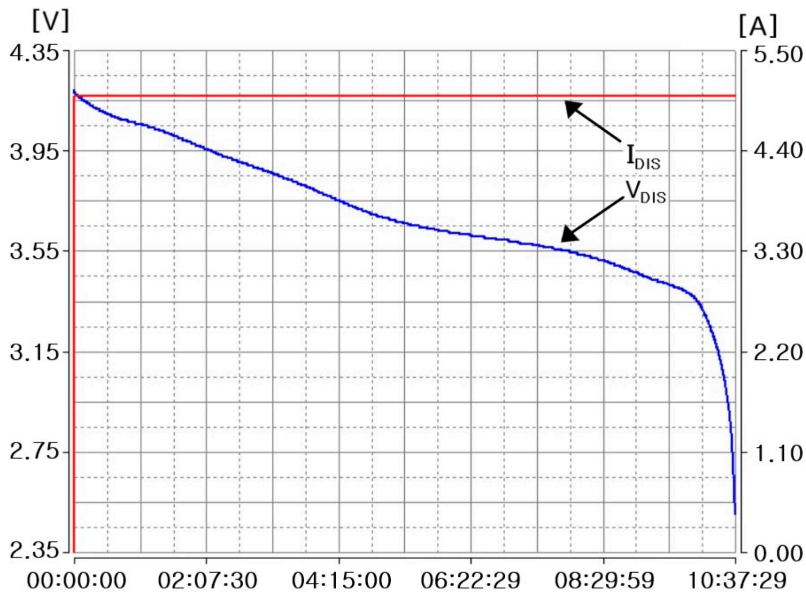

(**b**) Discharge voltage and current waveforms for a pouch-type Li-ion battery (Ⓐ Shenzhen Aoyouji Energy 50.5 Ah)

Figure 25. *Cont.*

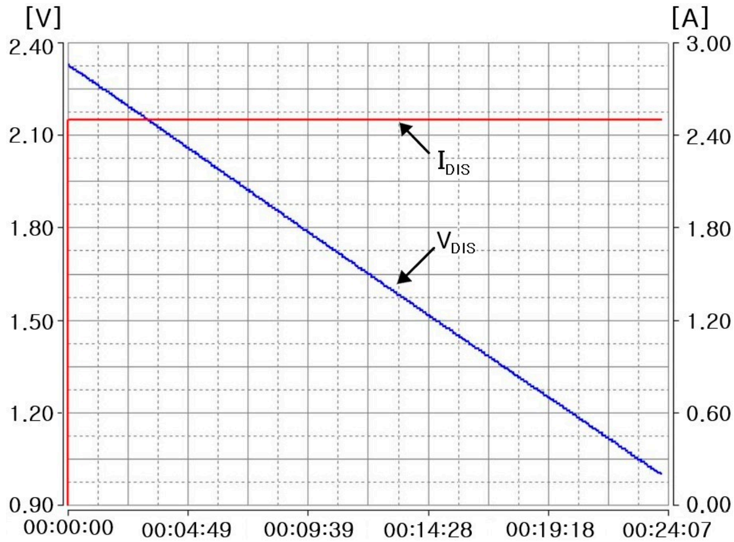

(**c**) Discharge voltage and current waveforms for a supercapacitor (Shenzhen Yedianxinbang 600 F)

Figure 25. Discharge voltage and current waveforms of Li-ion batteries and supercapacitor.

Figure 25a shows the discharge voltage and current waveforms when a cylindrical Li-ion battery (⑥ Samsung 2900 mAh) was discharged with a CC of 2.5 A.

The voltage of the battery gradually decreased from 4.2 to 3.15 V in about 60 min and then sharply decreased after 3.15 V.

Figure 25b shows the discharge voltage and current waveforms when a pouch-type Li-ion battery (Ⓐ Shenzhen Aoyouji Energy 50.5 Ah) was discharged with a CC of 5 A. The voltage of the battery gradually decreased from 4.2 to 3.35 V in about 10 h and then sharply decreased after 3.35 V.

Figure 25a,b shows the typical discharge characteristics of Li-ion batteries; the pouch-type Li-ion battery exhibited better energy storage characteristics than the cylindrical Li-ion battery.

Figure 25c shows the discharge voltage and current waveforms when the supercapacitor (Shenzhen Yedianxinbang 600 F) was discharged with a CC of 2.5 A. The voltage linearly decreased from 2.3 to 0.9 V in about 24 min. The discharge voltage and current waveforms verify that the characteristics of the supercapacitor are similar to those of an ideal energy storage device.

The fundamental reason for such a shape is indicated by the impedance spectrum curve. In the case of Li-ion batteries, the discharge voltage rapidly decreases when the state of charge (SOC) is low, but for supercapacitors, the slope of the discharge voltage is constant regardless of the SOC.

Currently, Li-ion batteries are widely used as energy storage systems (ESSs) and to power electric vehicles, and the Impedance Spectra method is expected to be very useful for quickly evaluating the performance of batteries and supercapacitors.

7. Conclusions

This study compared and analyzed 2600–3600 mAh 18650-type cylindrical Li-ion batteries, a 5000 mAh 21700-type cylindrical Li-ion battery, 37–50.5 Ah pouch-type Li-ion batteries, and a 600 F supercapacitor. Electrical and mathematical modeling was organized for the cylindrical and pouch-type Li-ion batteries and the supercapacitor. Subsequently, the impedance spectra of 13 types of 18650-type cylindrical Li-ion batteries, 1 type of 21700-type cylindrical Li-ion battery, 3 types of pouch-type Li-ion batteries, and 1 type of supercapacitor were obtained. For a cylindrical Li-ion battery, the R_S value of a battery with a protection device (circular thermal disc cap) is in the range of 14–38 mΩ. For the 18650-type cylindrical Li-ion battery with a protection device, the R_S value of the battery is between 48 and 105 mΩ, and the protection device increases the R_S value by at least 33 mΩ. A good Li-ion battery has small overall R_S, R_p, and C_p values. A cylindrical Li-ion battery exhibits a semicircular shape in the impedance spectrum, due to the oxidation and reduction reactions of Li ions, and the impedance increases with a slope of 45° in the complex plane, due to the Z_W generated by Li ion diffusion. However, for a pouch-type Li-ion battery, the impedance spectrum exhibits a part of the semicircular shape, due to the oxidation and reduction reactions of Li ions, and the Z_W generated by Li ion diffusion does not appear. In a supercapacitor, the oxidation and reduction reactions of ions do not appear at all, and the Z_W generated by Li ion diffusion does not occur. Thus, the impedance spectrum of a supercapacitor is very similar to that of an ideal capacitor. Therefore, the R_S values are in the order: 18650-type cylindrical Li-ion batteries >21700-type cylindrical Li-ion batteries > pouch-type Li-ion batteries > supercapacitor. Furthermore, when a Li-ion battery is discharged with CC, its voltage gradually decreases, up to a specific voltage, and then rapidly decreases. However, a supercapacitor has the characteristic of linearly discharging voltage during CC discharge. The study results are expected to be very useful for the performance analysis of electric vehicles, personal mobility, and ESS.

Funding: This research was funded by National Research Foundation of Korea(NRF) and the Ministry of Education(MOE): 2022RIS-002.

Data Availability Statement: Data sharing is not applicable.

Conflicts of Interest: The authors declare no conflict of interest.

References

1. Chan, H.L.; Sutanto, D. A New Battery Model for use with Battery Energy Storage Systems and Electric Vehicles Power Systems. In Proceedings of the IEEE Power Engineering Society Conference, Singapore, 23–27 January 2000; pp. 470–475. [CrossRef]
2. Sims, R.I.; Carnes, J.C.; Dzieciuch, M.A.; Fenton, J.E. *Computer Modeling of Automotive Lead Acid Batteries*; Ford Research Laboratories Technical Report; 1990; SR-90-154.
3. Ziyad, M.S.; Margaret, A.C.; William, A.L. A Mathematical Model for Lead-Acid Batteries. *IEEE Trans. Energy Con.* **1992**, *7*, 93–98. [CrossRef]
4. Margaret, A.C.; Ziyad, M.S. Determination of Lead-Acid Battery Capacity Via Mathematical Modeling Techniques. *IEEE Trans. Energy Con.* **1992**, *7*, 442–446. [CrossRef]
5. Buller, S.; Thele, M.; Doncker, R.W.D.; Karden, E. Impedance-Based Simulation Models of Supercapacitors and Li-Ion Batteries for Power Electronic Applications. *IEEE Trans. Ind. App.* **2005**, *41*, 742–747. [CrossRef]
6. Buller, S.; Karden, E.; Kok, D.; Doncker, R.W.D. Modeling the Dynamic Behavior of Supercapacitors Using Impedance Spectroscopy. *IEEE Trans. Ind. App.* **2002**, *38*, 1622–1626. [CrossRef]
7. Stroe, D.I.; Swierczynski, M.; Stan, A.I.; Knap, V.; Teodorescu, R.; Andreasen, S.J. Diagnosis of Lithium-Ion Batteries State-of-Health based on Electrochemical Impedance Spectroscopy Technique. In Proceedings of the IEEE Transactions on Energy Conversion Congress and Exposition (ECCE), Pittsburgh, PA, USA, 14–18 September 2014; pp. 4576–4582. [CrossRef]
8. Oldenburger, M.; Bedürftig, B.; Gruhle, A.; Grimsmann, F.; Richter, E.; Findeisen, R.; Hintennach, A. Investigation of the Low Frequency Warburg Impedance of Li-Ion Cells by Frequency Domain Measurements. *J. Energy Storage* **2019**, *21*, 272–280. [CrossRef]
9. Samuel, C.M.; Paul, G. An Impedance Model Based on a Transmission Line Circuit and a Frequency Dispersion Warburg Component for the Study of EIS in Li-Ion Batteries. *J. Electroanal. Chem.* **2020**, *871*, 114305. [CrossRef]
10. Maheshwari, A.; Heck, M.; Santarelli, M. Cycle Aging Studies of Lithium Nickel Manganese Cobalt Oxide-Based Batteries Using Electrochemical Impedance Spectroscopy. *Electrochim. Acta* **2018**, *273*, 335–348. [CrossRef]
11. Karden, E.; Buller, S.; Doncker, R.W.D. A Frequency-Domain Approach to Dynamical Modeling of Electrochemical Power Sources. *Electrochim. Acta* **2002**, *47*, 2347–2356. [CrossRef]
12. Buller, S.; Thele, M.; Karden, E.; Doncker, R.W.D. Impedance-Based Non-Linear Dynamic Battery Modeling for Automotive Applications. *J. Power Source* **2003**, *113*, 422–430. [CrossRef]
13. Chen, M.; Rincón-Mora, G.A. Accurate Electrical Battery Model Capable of Predicting Runtime and I–V Performance. *IEEE Trans. Energy Con.* **2006**, *21*, 504–511. [CrossRef]
14. Lee, J.M.; Nam, O.Y.; Cho, B.H. Li-ion Battery SOC Estimation Method Based on the Reduced Order Extended Kalman Filtering. *J. Power Source* **2007**, *174*, 9–15. [CrossRef]
15. Kim, J.H.; Shin, J.W.; Chun, C.Y.; Cho, B.H. Stable Configuration of a Li-Ion Series Battery Pack Based on a Screening Process for Improved Voltage/SOC Balancing. *IEEE Trans. Power Electron.* **2012**, *27*, 411–424. [CrossRef]
16. Deng, Z.; Zhang, Z.; Lai, Y.; Liu, J.; Li, J.; Liu, Y. Electrochemical Impedance Spectroscopy Study of a Lithium/Sulfur Battery: Modeling and Analysis of Capacity Fading. *J. Electrochem. Soc.* **2013**, *160*, A553–A558. [CrossRef]

17. Bugryniec, P.J.; Davidson, J.N.; Brown, S.F. Advanced Abuse Modelling of Li-ion Cells—A Novel Description of Cell Pressurisation and Simmering Reactions. *J. Power Source* **2020**, *474*, 228396. [CrossRef]
18. Abada, S.; Marlair, G.; Lecocq, A.; Petit, M.; Sauvant-Moynot, V.; Huet, F. Safety Focused Modeling of Lithium-Ion Batteries: A Review. *J. Power Source* **2016**, *306*, 178–192. [CrossRef]
19. Gauchia, L.; Castaño, S.; Sanz, J. New Approach to Supercapacitor Testing and Dynamic Modelling. In Proceedings of the IEEE, Vehicle Power and Propulsion Conference, Lille, France, 1–3 September 2010; pp. 1–5. [CrossRef]
20. Mahon, P.J.; Paul, G.L.; Keshishian, S.M.; Vassallo, A.M. Measurement and Modelling of the High-Power Performance of Carbon-Based Supercapacitors. *J. Power Source* **2000**, *91*, 68–76. [CrossRef]
21. Du, Y.; Mo, Y.; Chen, Y. Effects of Fe Impurities on Self-Discharge Performance of Carbon-Based Supercapacitors. *Materials* **2021**, *14*, 1908. [CrossRef] [PubMed]
22. Himanshu; Rao, S.S.; Punnoose, D.; Sathishkumar, P.; Gopi, C.V.V.M.; Bandari, N.; Durga, I.K.; Krishna, T.N.V.; Kim, H.J. Development of Novel and Ultra-High-Performance Supercapacitor Based on a Four Layered Unique Structure. *Electronics* **2018**, *7*, 121. [CrossRef]
23. Huang, Z.; Qin, C.; Wang, J.; Cao, L.; Ma, Z.; Yuan, Q.; Lin, Z.; Zhang, P. Research on High-Value Utilization of Carbon Derived from Tobacco Waste in Supercapacitors. *Materials* **2021**, *14*, 1714. [CrossRef]
24. Yuan, Y.; Sun, Y.; Feng, Z.; Li, X.; Yi, R.; Sun, W.; Zhao, C.; Yang, L. Nitrogen-doped hierarchical porous activated carbon derived from paddy for high-performance supercapacitors. *Materials* **2021**, *14*, 318. [CrossRef]
25. Khalid, S.; Cao, C.; Naveed, M.; Younas, W. 3D hierarchical MnO_2 microspheres: A prospective material for high performance supercapacitors and lithium-ion batteries. *Sustain. Energy Fuels* **2017**, *1*, 1795–1804. [CrossRef]
26. Bi, S.; Banda, H.; Chen, M.; Niu, L.; Chen, M.; Wu, T.; Wang, J.; Wang, R.; Feng, J.; Chen, T.; et al. Molecular understanding of charge storage and charging dynamics in supercapacitors with MOF electrodes and ionic liquid electrolytes. *Nat. Mater.* **2020**, *19*, 552–558. [CrossRef]
27. Stroe, D.I.; Knap, V.; Swierczynski, M.; Schaltz, E. Electrochemical Impedance Spectroscopy-based Electric Circuit Modeling of Lithium-Sulfur Batteries during Discharging State. *IEEE Trans. Ind. Appl.* **2019**, *55*, 631–637. [CrossRef]
28. Lee, J.H.; Choi, W.J. Novel State-of-Charge Estimation Method for Lithium Polymer Batteries Using Electrochemical Impedance Spectroscopy. *J. Power Electron.* **2011**, *11*, 237–243. [CrossRef]
29. Sihvo, J.; Stroe, D.I.; Messo, T.; Roinila, T. A Fast Approach for Battery Impedance Identification Using Pseudo Random Sequence (PRS) Signals. *IEEE Trans. Power Electron.* **2020**, *35*, 2548–2557. [CrossRef]
30. Santoni, F.; Angelis, A.D.; Moschitta, A.; Carbone, P. Digital Impedance Emulator for Battery Measurement System Calibration. *Senors* **2021**, *21*, 7377. [CrossRef] [PubMed]
31. Islam, S.M.R.; Park, S.Y.; Balasingam, B. Unification of Internal Resistance Estimation Methods for Li-Ion Batteries Using Hysteresis-Free Equivalent Circuit Models. *Batteries* **2020**, *6*, 32. [CrossRef]
32. Ovejas, V.J.; Cuadras, A. Impedance Characterization of an LCO-NMC/Graphite Cell: Ohmic Conduction, SEI Transport and Charge-Transfer Phenomenon. *Batteries* **2018**, *4*, 43. [CrossRef]
33. Gheem, E.V.; Pintelon, R.; Vereecken, J.; Schoukens, J.; Hubin, A.; Verboven, P.; Blajiev, O. Electro-Chemical Impedance Spectroscopy in the Presence of Nonlinear Distortions and Non-Stationary Behaviour Part I: Theory and Validation. *Electrochim. Acta* **2004**, *49*, 4753–4762. [CrossRef]
34. Kim, J.H.; Kowal, J. Development of a Matlab/Simulink Model for Monitoring Cell State-of-Health and State-of-Charge via Impedance of Lithium-Ion Battery Cells. *Batteries* **2022**, *8*, 8. [CrossRef]
35. Heinrich, M.; Wolff, N.; Seitz, S.; Krewer, U. Identifying Anode and Cathode Contributions in Li-Ion Full-Cell Impedance Spectra. *Batteries* **2022**, *8*, 40. [CrossRef]
36. Goldammer, E.; Kowal, J. Determination of the Distribution of Relaxation Times by Means of Pulse Evaluation for Offline and Online Diagnosis of Lithium-Ion Batteries. *Batteries* **2021**, *7*, 36. [CrossRef]
37. Macdonald, J.R. Impedance Spectroscopy. *Ann. Biomed. Eng.* **1992**, *20*, 289–305. [CrossRef] [PubMed]
38. Choi, W.S.; Shin, H.C.; Kim, J.M.; Choi, J.Y.; Yoon, W.S. Modeling and Applications of Electrochemical Impedance Spectroscopy (EIS) for Lithium-ion Batteries. *J. Electrochem. Sci. Technol* **2020**, *11*, 1–13. [CrossRef]
39. Olarte, J.; Ilarduya, J.M.; Zulueta, E.; Ferret, R.; Fernández-Gámiz, U.; Lopez-Guede, J.M. A Battery Management System with EIS Monitoring of Life Expectancy for Lead–Acid Batteries. *Electronics* **2021**, *10*, 1228. [CrossRef]
40. Franke-Lang, R.; Kowa, J. Analysis of Electrochemical Impedance Spectroscopy on Zinc-Air Batteries Using the Distribution of Relaxation Times. *Batteries* **2021**, *7*, 56. [CrossRef]
41. Podias, A.; Pfrang, A.; Persio, F.D.; Kriston, A.; Bobba, S.; Mathieux, F.; Messagie, M.; Boon-Brett, L. Sustainability Assessment of Second Use Applications of Automotive Batteries: Ageing of Li-Ion Battery Cells in Automotive and Grid-Scale Applications. *World Electr. Veh. J.* **2018**, *9*, 24. [CrossRef]
42. Hasan, R.; Scott, J. Impedance Measurement of Batteries under load. In Proceedings of the IEEE International Instrumentation and Measurement Technology Conference(I2MTC), Auckland, New Zealand, 20–23 May 2019. [CrossRef]
43. Ray, A.; Saruhan, B. Application of Ionic Liquids for Batteries and Supercapacitors. *Materials* **2021**, *14*, 2942. [CrossRef]
44. Yang, G.; Song, Y.; Wang, Q.; Zhang, L.; Deng, L. Review of ionic liquids containing, polymer/inorganic hybrid electrolytes for lithium metal batteries. *Mater. Des.* **2020**, *190*, 108563. [CrossRef]

45. Karuppasamy, K.; Theerthagiri, J.; Vikraman, D.; Yim, C.J.; Hussain, S.; Sharma, R.; Maiyalagan, T.; Qin, J.; Kim, H.S. Ionic liquid-based electrolytes for energy storage devices: A brief review on their limits and applications. *Polymers* **2020**, *12*, 918. [CrossRef]
46. Zhang, R.; Xia, B.; Li, B.; Cao, L.; Lai, Y.; Zheng, W.; Wang, H.; Wang, W. State of the Art of Lithium-Ion Battery SOC Estimation for Electrical Vehicles. *Energies* **2018**, *11*, 1820. [CrossRef]
47. Rivera-Barrera, J.P.; Muñoz-Galeano, N.; Sarmiento-Maldonado, H.O. SoC Estimation for Lithium-ion Batteries: Review and Future Challenges. *Electronics* **2017**, *6*, 102. [CrossRef]
48. Hahn, M.; Schindler, S.; Triebs, L.C.; Danzer, M.A. Optimized Process Parameters for a Reproducible Distribution of Relaxation Times Analysis of Electrochemical Systems. *Batteries* **2019**, *5*, 43. [CrossRef]